Unitary Conductance Variation in Kir2.1 and in Cardiac Inward Rectifier Potassium Channels

Arturo Picones,* Edmund Keung,† and Leslie C. Timpe†
*Department of Physiology, University of California–San Francisco, San Francisco, California 94143; and †Section of Cardiology, Department of Veterans Affairs Medical Center, San Francisco, California 94121 USA

ABSTRACT Kir2.1 (IRK1) is the complementary DNA for a component of a cardiac inwardly rectifying potassium channel. When Kir2.1 is expressed in *Xenopus* oocytes or human embryonic kidney (HEK) cells (150 mM external KCl), the unitary conductances form a broad distribution, ranging from 2 to 33 pS. Channels with a similarly broad distribution of unitary conductance amplitudes are also observed in recordings from adult mouse cardiac myocytes under similar experimental conditions. In all three cell types channels with conductances smaller, and occasionally larger, than the ~30 pS ones are found in the same patches as the ~30 pS openings, or in patches by themselves. The unitary conductances in patches with a single active channel are stable for the durations of the recordings. Channels of all amplitudes share several biophysical characteristics, including inward rectification, voltage sensitivity of open probability, sensitivity of open probability to external divalent cations, shape of the open channel *i-V* relation, and Cs^+ block. The only biophysical difference found between large and small conductance channels is that the rate constant for Cs^+ block is reduced for the small-amplitude channels. The unblocking rate constant is similar for channels of different unitary conductances. Apparently there is significant channel-to-channel variation at a site in the outer pore or in the selectivity filter, leading to variability in the rate at which K^+ or Cs^+ enters the channel.

INTRODUCTION

It has been assumed in theoretical descriptions of ion channel kinetics that channels of the same type exhibit the same unitary conductance (Katz and Miledi, 1972; Anderson and Stevens, 1973; Conti and Wanke, 1975; Neher and Stevens, 1977; Colquhoun and Hawkes, 1977). This idea has survived the development of methods that allow single open channels to be studied, the lipid bilayer and patch clamp recording techniques, with only a few exceptions. Subconductance states accessed from the main open state were recognized in early patch clamp experiments (Fox, 1987). There are also examples of subconductance states that are visited from the closed state, rather than the main open state, in glycine- and glutamate-activated channels (Hamill et al., 1983; Cull-Candy and Usowicz, 1987; Jahr and Stevens, 1987). In these cases, however, it is possible to identify a main open state as the most frequently observed open state. The experiments to be described here were motivated by the observation that a cloned inward rectifier K^+ channel, mouse Kir2.1 (IRK1), displays unitary conductances ranging continuously from 2 to 33 pS when the cDNA is expressed in *Xenopus* oocytes or human embryonic kidney (HEK) cells. This was a surprising observation, and the possibility had to be considered that some of the channels were background channels in the expression systems, rather than being Kir2.1 channels. A series of biophysical experiments was therefore carried out to clarify the relationship between the larger and smaller channels, and to identify any differences that might suggest a reason for the variation in current amplitudes.

The Kir2.1 gene is expressed in the heart, to a greater extent in the ventricles than in the atria, and its product is one component of the constitutively activated inward rectifier of ventricular myocytes, I_{K1} (Kubo et al., 1993; Ishihara and Hiraoka, 1994; Plaster et al., 2001; Zaritsky et al., in press). A number of studies have reported heterogeneity in the unitary conductances of I_{K1} channels in the heart, and also in corneal epithelial cells, which likewise express Kir2.1 (see Discussion). The variation in unitary conductance amplitudes observed in those older experiments on native channels could have been explained by the presence of more than one inward rectifier (Kir) channel type in myocytes or corneal epithelial cells. The result reported here, that Kir2.1 expressed heterologously gives rise to channels with a broad range of unitary conductances, suggests an alternative explanation: Kir2.1 may be the predominant Kir gene expressed in cardiac myocytes, and the variation in unitary conductances would be similar to that found in heterologous expression experiments. The Kir2.1 cDNA clone used in the experiments to be described is a mouse clone (Kubo et al., 1993). We therefore examined the distribution of unitary conductances in mouse cardiac myocytes to determine whether a similarly broad range of unitary conductances was present when the Kir2.1 gene is expressed in its native cell type and species.

Received for publication 23 October 2000 and in final form 13 July 2001.
Address reprint requests to Dr. Leslie C. Timpe, 1429 Cabrillo Ave., Burlingame, CA 94010. Tel.: 650-342-8737; Fax: 415-750-6633; E-mail: lct@itsa.ucsf.edu.

0006-3495/01/10/2035/15 $2.00

MATERIALS AND METHODS

Oocyte expression

Oocytes were obtained from *Xenopus laevis* frogs under tricaine anesthesia. Kir2.1 cRNA was synthesized from the cDNA clone isolated by Kubo

et al. (1993) in a standard in vitro transcription reaction that included the cap analog $m^7G(5')ppp(5')G$ (Ambion; Austin, TX) at a ratio of 4:1 cap analog/GTP. The cDNA template was digested with RQ1 DNAse (Promega; Madison, WI), and the reaction extracted with 1:1 phenol/chloroform. The cRNA was then precipitated with 7.5 M LiCl and 50 mM EDTA, and taken up in distilled water. Fifty nanoliters of cRNA injected at 13 ng/μl (as determined by spectrophotometry) gave an expression level suitable for single channel experiments. One day after oocyte injection the adhering epithelium was loosened by incubation for 1 h in 1 mg/ml collagenase (type 1A, Sigma; St. Louis, MO). In most experiments the vitelline membrane was removed using a hypertonic saline, as described by Methfessel et al. (1986). The recordings were made two or three days after injection.

Functional expression in HEK cells

The mammalian cell line tsA-201, a subclone of HEK 293, was maintained in DME H21/F12 medium and passaged twice a week. The cells were plated on poly-L-lysine coated glass coverslips and were transfected with 2–10 μg/ml Kir2.1 cDNA (in the pcDNA 1 vector, Invitrogen, San Diego, CA), with 8 μg/ml of a plasmid carrying SV40 T antigen, and with a plasmid bearing enhanced Green Fluorescent Protein (eGFP) using the calcium phosphate method. Co-transfection with eGFP allowed the cells expressing Kir2.1 at a high level to be identified using epifluorescence. Experiments were carried out 24–48 h after transfection. The bath and pipette saline solutions were the same as those used for the oocyte recordings.

Isolation of cardiac myocytes

Male mice were anesthetized with intraperitoneal pentobarbitol (0.1 ml of a 50 mg/ml solution), and the hearts were excised in 45 s or less and attached to a Langendorff apparatus. The hearts were then perfused retrogradely with nominally Ca^{2+}-free Tyrode's solution at pH 7.3, saturated with 100% O_2 at 35°. Solutions were gassed continuously during the procedure. After 5 min of 0 Ca^{2+} perfusion, the heart was perfused with the same solution containing 1.0 mg/ml collagenase (type B, Boehringer-Mannheim/Roche Molecular Biochemicals; Mannheim, Germany). Up to 50 μM $CaCl_2$ was sometimes used to increase enzymatic activity.

After 12 min the hearts were decannulated, placed in a dish with fresh collagenase solution, and teased apart. The resulting suspension was filtered through a cell culture "cellector" (Bellco; Vineland, NJ). The cells were pelleted at a very low rotational speed, the collagenase solution removed, and the cells were washed once in zero Ca^{2+} Tyrode's and twice with a modified Kraft-Bruhe (KB) saline that contained (in mM): 70 potassium glutamate, 25 KCl, 10 KH_2PO_4, 10 oxalic acid, 10 taurine, 11 glucose, 2 pyruvic acid, 2 K-ATP, 2 creatine phosphate, 10 Hepes (pH 7.2) 5 $MgCl_2$. After the final wash the myocytes were allowed to settle by gravity for 5 min., then removed and placed into a dish containing fresh KB solution. The isolated cells were maintained at room temperature, and the experiments performed on the day of isolation. Cell-attached patches were made using KB saline in the experimental chamber.

Electrophysiology

Patch pipettes were fabricated from aluminosilicate or borosilicate glass (Garner Glass, Claremont, CA), and coated with Sylgard (Dow Corning; Midland, MI). The experiments were conducted and analyzed using pCLAMP 7 programs and Axon Instruments amplifiers (Axopatch-1D or Axopatch 200A, Axon Instruments, Foster City, CA). Long-duration recordings were stored unfiltered on VHS tape. The signals were subsequently filtered (−3 dB) at 1.5 kHz using an eight-pole Bessel filter and then digitized at 5 kHz for the time domain analysis. Oversampling by a factor of ~3 is recommended for mean variance analysis (Patlak, 1993). The saline solution in the experimental chamber contained (in mM): 140 KCl, 7 $MgCl_2$, 1 $CaCl_2$, 5 Hepes at pH 7.4. The standard pipette solution contained (in mM): 150 KCl, 1 $CaCl_2$, 5 Hepes at pH 7.4. The divalent cation free pipette saline contained (in mM): 150 KCl, 1 EDTA, 1 EGTA, and 5 Hepes at pH 7.4. The experiments were carried out at room temperature. The mean-variance histograms (MVH) in the figures were prepared using a window width of 100 sample points. The precision is reported as the standard deviation of the window means. The MVH program was obtained from Dr. Joseph Patlak at http://salus.med.uvm.edu/~patlak/.

Analysis of current fluctuations in single open channels

Block of the Kir2.1 channel by Cs^+ was studied in cell-attached patches by adding 10 μM Cs^+ to the standard pipette saline. For the spectral density distribution analysis the current traces were filtered at 10 kHz with a eight-pole Butterworth analog filter (Frequency Devices, Haverhill, MA) and then digitized at 25 kHz. The current records were divided into 350-ms sections of closed channel or open channel to calculate the spectral density function. The difference spectra were calculated from open and nearby closed channel data from the same patch. The final, plotted, spectrum was computed from the average of three differential spectra obtained in a similar fashion. For the graphic display of the spectral density distribution data, points below 50 Hz are individual data points, points between 50 and 500 Hz are the average of two consecutive data points, and those between 500 and 5000 Hz are the average of 10 consecutive data points. Equation 8 was fit to the data using a nonlinear least-squares fitting algorithm.

RESULTS

Initially, Kir2.1 channels were studied using the *Xenopus* oocyte expression system (Kubo et al., 1993). Currents through one or a small number of Kir2.1 channels in the membrane of the oocyte were characterized by patch electrode recordings in the cell-attached configuration. High potassium saline solutions were present in the pipette, and also in the experimental chamber, to set the intracellular potential near 0 mV. Fig. 1 *A* shows three examples of current records obtained from a patch containing a single active Kir2.1 channel. Stepping the membrane potential from 0 mV to −80 mV activates the channel, which then inactivates spontaneously. The ensemble average (Fig. 1 *B*) and the individual current traces show that, following the peak of inward current, there is a significant probability that a channel will reopen, leading to a steady-state current. Fig. 1 *C* is from a recording of a freshly isolated mouse cardiac myocyte made under conditions similar to those in the oocyte recording. The patch contained two active channels. The mouse channels likewise activate transiently in response to steps from 0 to −80 mV. The unitary current amplitudes and the time constants of inactivation, 243 and 308 ms for the Kir2.1 and myocyte channels, respectively, are comparable, as expected if the Kir2.1 channel and the native inward rectifier channel are structurally similar or identical. These examples illustrate a unitary conductance amplitude (27.1 pS for Kir2.1 and 33.1 pS for the cardiac channels, recorded with 150 mEq K^+ in the pipette) which

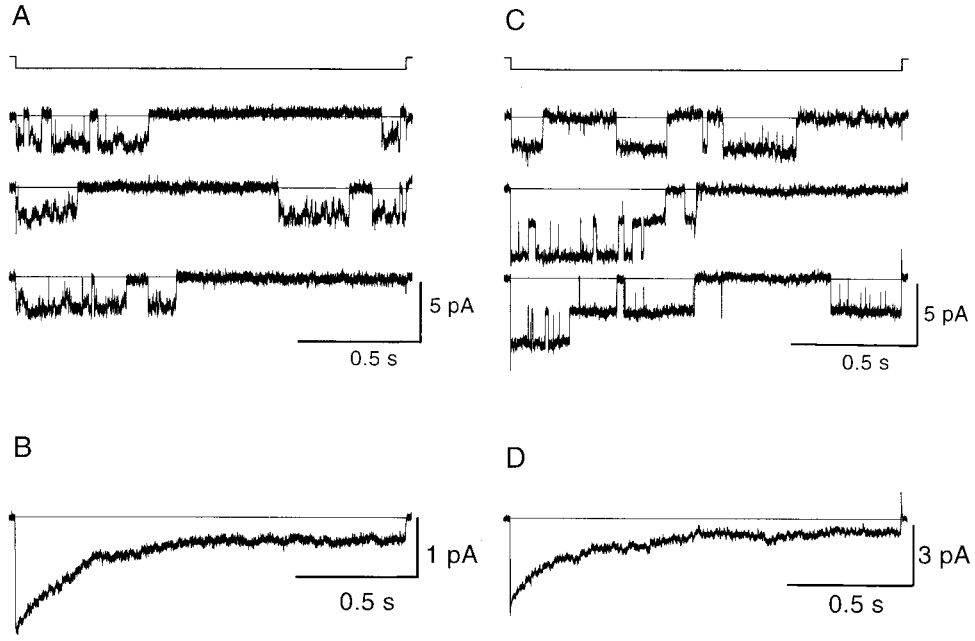

FIGURE 1 Single inwardly rectifying potassium channel currents recorded in a *Xenopus* oocyte expressing Kir2.1 and in a freshly dissociated mouse cardiac myocyte. (*A*) Cell-attached current recordings of an oocyte membrane patch containing one active channel. Current traces are in response to voltage steps to −80 mV from a holding voltage of 0 mV (*upper trace*). (*B*) Ensemble average of 262 traces from the patch of (*A*) showing time-dependent inactivation that can be described by exponential decay with a time constant of 243 ms. (*C*) Cell-attached current recordings from a mouse myocyte membrane patch containing two channels. The pulse protocol was the same as in (*A*). (*D*) Ensemble average of 162 similar current traces showing time-dependent inactivation characterized by exponential decay with a time constant of 308 ms. The closed channel current level in this and other figures is indicated by the continuous lines.

is similar to those found in rodent hearts by other laboratories (see Discussion).

Examination of the Kir2.1 currents in other patches shows that openings of more than one amplitude are often present (Fig. 2 *A*). In this example two current amplitudes were observed, a larger one of 2.49 pA and a smaller one of 0.44 pA. Neither current size was observed in control, water-injected oocytes studied under the same conditions (9 patches in 5 oocytes). Control oocytes sometimes did exhibit openings from an endogenous stretch-activated channel. The stretch-activated channels were readily distinguished from Kir2.1 channels by their greater current amplitudes and flickery openings. Currents through large and small Kir2.1 channels were not seen near 0 mV, or at more positive potentials, and thus all displayed inward rectification.

The amplitudes of the different currents were stable for the length of the patch recordings. Fig. 2 *D* (*solid line*) shows an all points histogram taken from a short section of data near the beginning of the experiment of Fig. 2 *A*, and also a histogram from near the end of the experiment (*dotted line*). Peaks corresponding to the small (0.44 pA) and large (2.49 pA) channels are clearly present, and have very similar amplitudes. In patches with both large and small channels the open times would occasionally overlap. When this occurred the currents summed, as seen near the end of the third trace in Fig. 2 *A*. The overlap is also apparent as a small peak at around 3 pA in the histograms (Fig. 2 *D*). The mean variance histogram (MVH) provides a method to summarize long episodes of single channel data (Patlak, 1993). Fig. 2 *E* displays the MVH for 138 s of recording time from the patch of part *A*. The peak corresponding to the small open level is clearly separated from the much larger peak associated with the closed state. The more negative peak, corresponding to the large open level, is asymmetrical due partly to the simultaneous openings of the large and small channels.

We used the MVH to summarize recordings of several minutes' duration, and also to measure channel open probability. The amplitudes of many of the unitary currents observed here were small enough that the standard idealization procedure (using a 50% threshold for detecting transitions) was not suitable for measuring the open probability (Colquhoun and Sigworth, 1995). In Fig. 2 *A*, for example, the ratio of the current mean to the standard deviation of the open channel is ~9.6 for the large open level and 2.4 for the small one. Open probability (P_o) was determined instead using the MVH, which performs well on data with a signal-to-noise ratio as low as two (Patlak, 1993). For the large opening of Fig. 2 *A*, P_o determined from idealized data using the 50% criterion was 0.11, whereas P_o determined from the MVH was 0.12. In a sample of eight patches in

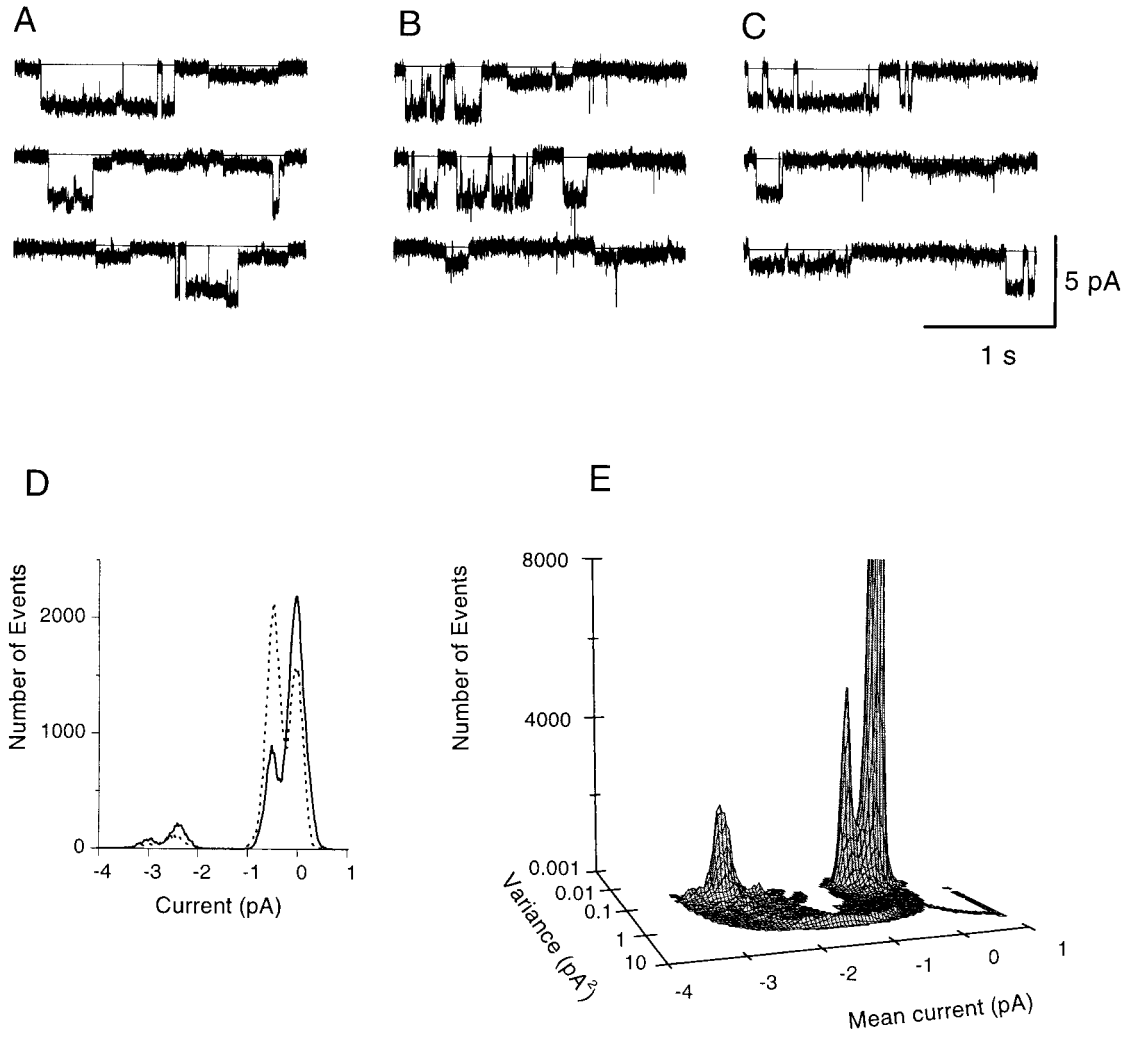

FIGURE 2 Patches from *Xenopus* oocytes and HEK cells expressing Kir2.1, and from mouse cardiac myocytes, contain small and large channel openings. (*A*) Oocyte recording at −80 mV. The traces show openings to two different conductance levels and closings to at least one subconductance level. (*B*) Current traces obtained from a mouse cardiac myocyte under similar conditions as in (*A*). Large and small openings are both present. The large channel visits several subconductance states. (*C*) Kir2.1 channel activity recorded from a transfected HEK cell at −80 mV. The current traces show channel openings to two distinct current levels. (*D*) All points histograms from the same patch as in (*A*). The recording lasted 180 s. The solid curve corresponds to a histogram made from 10 s of data beginning at 32 s into the recording; the dotted curve corresponds to 10 s starting at 151 s. (*E*) The MV histogram was obtained from 138 s of recording from the patch in (*A*). The three distinct peaks derive from the closed state (peak centered around 0 pA) and from two conducting levels with mean amplitudes of −0.44 ± 0.074 pA and −2.49 ± 0.122 pA. These means correspond to chord conductance values of 5.5 and 31.1 pS.

which the signal-to-noise ratio was large enough to permit idealization, the average P_o at −80 mV was estimated as 0.16 ± 0.10 (SD) using idealized data and 0.16 ± 0.13 (SD) using the MVH. The MVH method is thus quite reliable for these data, and allowed the open probabilities to be measured at the same bandwidth over a large range of channel conductances. The open probabilities for the small and large channels in Fig. 2 *A* were 0.14 and 0.12, respectively.

Large and small inward rectifier channels were also observed in freshly dissociated mouse cardiac myocytes. Fig. 2 *B* shows an example with a main current level of ~2.5 pA, and also a smaller current similar to those seen in the oocyte recordings. Similar findings for inward rectifier channels in cardiac myocytes of other species have been reported by other laboratories (see Discussion). The open state of the large channel is noisy, due to unresolved closures or visits to a subconductance state; there are also a few resolved visits to subconductance states. Human embryonic kidney cells co-transfected transiently with Kir2.1 and eGFP likewise expressed both large and small conductance channels. An example is shown in Fig. 2 *C*. These channels also displayed a broad range of conductances, ranging from 7 to 33 pS. Ensemble averages from patches with one or a few channels show inactivation similar to that of channels in

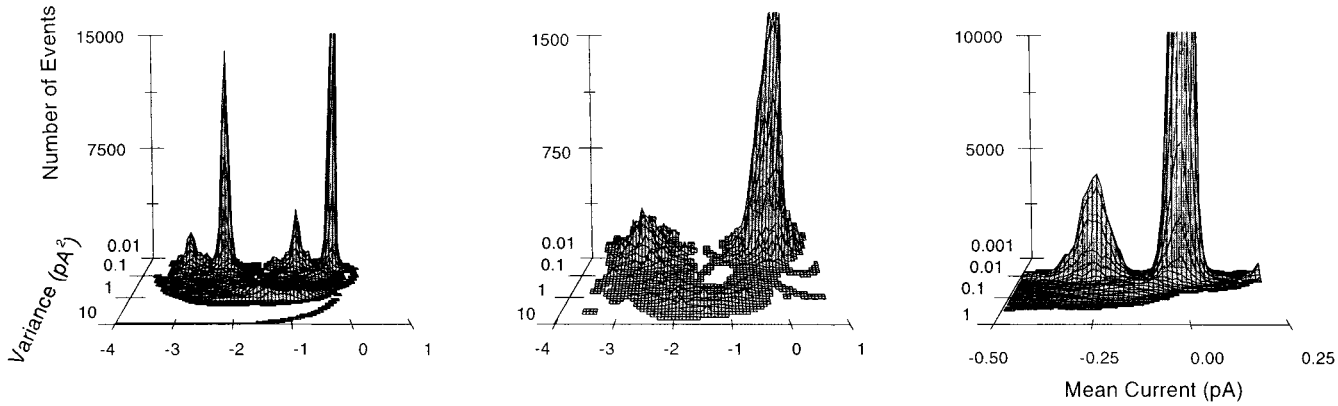

FIGURE 3 Examples of the distribution of open levels in oocyte patches. All the currents were recorded at −80 mV. A: membrane patch containing two open levels. The most common mean currents (maximum values depicted by the peaks) are −0.77 ± 0.096 and −2.29 ± 0.0937 pA, which correspond to conductances of 9.6 and 28.6 pS, respectively. The leftmost peak at −3.1 pA is the superposition of both current levels. For this MV histogram a total of 172 s of recording were analyzed. The estimated open probabilities are 0.14 and 0.35 for the small and the large conductance channels, respectively. B: patch containing a single large conductance channel. The mean current was −2.67 ± 0.012 pA, corresponding to 33.4 pS; P_o = 0.13. These estimates were derived from a total of 32 s of data. C: patch that included a single small opening (3.3 pS corresponding to the peak at −0.26 ± 0.078 pA in the MVH plot). The P_o, 0.14, was measured from 302 s of recording.

oocytes or mouse cardiac myocytes (Fig. 6 *C*). Human embryonic kidney cells lacking eGFP fluorescence, which were presumably not transfected by Kir2.1, did not display large or small Kir2.1 channel activity (five patches). The HEK cells have endogenous ion channels, including K^+ channels, but these have much larger unitary conductances and obviously different gating kinetics than Kir2.1 (Zhu et al., 1998).

Patches with one large and one small channel were observed frequently, although patches with only a large channel or only a small one were also found (Fig. 3). To increase the chance of obtaining patches with exactly one active channel, Kir2.1 mRNA was injected into oocytes at a concentration that gave a significant number of patches with no Kir2.1 channel activity (see Methods). Over the entire study, the fraction of empty patches was ~50%. Nevertheless, patches that displayed two openings of different amplitudes were frequently observed (Fig. 3, A), as well as patches with single active channels that could have any amplitude conductance, e.g., large (Fig. 3, B) or small (Fig. 3, C). In a set of 27 patches that contained no more than two different conductance levels, 12 patches had both large and small channels, 15 had only one conductance size. In the set of single channel patches the conductance level was stable throughout the duration of the experiment, which was tens of minutes in favorable cases.

There is considerable variation in the amplitudes of the unitary conductances in both Kir2.1 channels and in Kir channels in cardiac myocytes. Fig. 4 *A* displays a histogram of conductances measured in oocytes (*filled bars*) and myocytes (*hatched bars*). The conductances range from 2 to 33 pS in oocytes and from 4 to 41 pS in cardiac myocytes. Some of this variation is due to experimental or sampling errors, but much of it reflects real differences in unitary conductances. The current measurements from which the conductances were calculated were obtained from MV histograms, and are the average values from tens of seconds to several minutes of stable recording time. In Fig. 2 *E* the means entered into the histogram are the average of 100 consecutive data points. The standard deviation of the means for the large conductance channel is 0.122 pA. This value corresponds to 1.5 pS at −80 mV, and is less than the binwidth in the histogram of Fig. 4 *A*. Thus most of the variation in Fig. 4 *A* must result from real differences in unitary current amplitude, rather than sampling error.

Sakmann and Trube (1984a) and Matsuda (1988) have proposed that the Kir channel of guinea pig ventricular myocytes comprises three or four parallel conducting barrels or protochannels, which generally open and close together. The small conductance levels described here might then be due to one or two protochannels opening independently. There is a suggestion of peaks in the 25–30 pS and 5–10 pS bins in the histogram of Fig. 4 *A*, but peaks might be obscured by small differences in conditions or patch geometry from experiment to experiment. Fig. 4 *B* shows the relative amplitudes of large and small channels observed in a set of 36 recordings in which both channels were present. Recordings made at −60, −80, −100, or −120 mV are identified by different symbols. The ratio of small to large currents in the same patch is plotted as a function of the larger unitary conductance. The observations do not fall consistently near 0.25 or 0.33, as expected if the small opening in a patch were due to the opening of one of three or four protochannels.

If channels whose conductances are distributed as in Fig. 4 *A* were structurally independent, and were sampled ran-

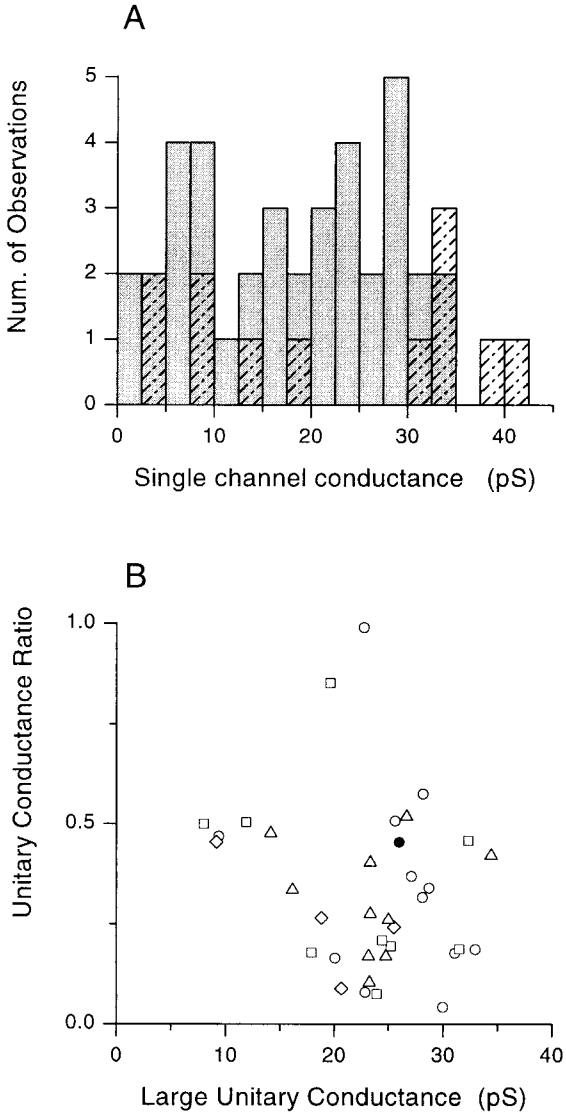

FIGURE 4 Kir2.1 and mouse cardiac Kir channels have a broad distribution of unitary conductance values. (*A*) Histogram of chord conductances of Kir2.1 channels measured at −80 mV. The data were obtained from 39 channels recorded in 27 different membrane patches, 12 of which had channels of two different conductance values. The distribution of conductance amplitudes for Kir channels recorded in mouse cardiac myocytes, also at −80 mV, is represented by the hatched bars (12 channels recorded from 7 different patches, 5 of which had channels of two different conductances). (*B*) Comparison of large and small open levels recorded in patches with two open levels. The ratio of the small to large open level is plotted as a function of the unitary conductance of the large open level. Each symbol corresponds to one patch. The different symbols identify measurements made at different patch potentials: *triangles*, −120 mV; *squares*, −100 mV; *circles*, −80 mV; *diamonds*, −60 mV. The 26 open symbols are from oocyte patches, and the filled circle is from a HEK cell patch.

domly by the patch pipette, then recordings with two channels should be more uniformly distributed than they are in Fig. 4 *B*. Recordings with two large channels, for example, or recordings with two smaller channels of similar size, should be found fairly frequently and should be represented

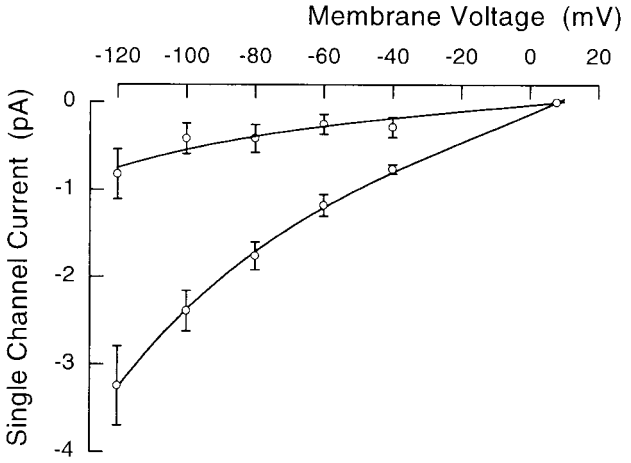

FIGURE 5 Current-to-voltage (*i-V*) relationships for large and small Kir2.1 channels expressed in oocytes; $n = 7$ for each point. Vertical bars are ± SEM. The solid lines were plotted from a single barrier permeation model (Eq. 1 in the text) using the parameters $B = 3.38$ pS and $s = 0.39$ for the large open values, and $B = 0.77$ pS and $s = 0.40$ for the small levels.

by points in the upper right and upper left quadrants, respectively. Only the lower left quadrant would be underpopulated, due to the limit on resolving small currents. The recordings plotted in Fig. 4 *B* were selected for the presence of two active channels, not for those channels' sizes. The clustering in the lower righthand quadrant, therefore, indicates a tendency for large and small conductance openings to appear together in the same patch. This finding suggests that the large and small openings may result from the activity of a channel complex. In comparing biophysical properties we often describe the channels as "large" or "small," reflecting the fact that one large and one small channel often do appear together. There is no natural partition of the channels into two size groups, however, as is apparent from the histogram in Fig. 4 *A*.

Voltage dependence of current amplitude and open probability

Open levels were sorted somewhat arbitrarily into two pools, with large (16–30 pS) or small (2–9 pS) unitary conductances, for the purpose of comparing *i-V* characteristics and open probability. The current through both the large and small open levels displays inward rectification between −40 and −120 mV (Fig. 5). An attempt was made to fit the *i-V* data using the Goldman current equation. With 150 mM KCl for the extracellular $[K^+]$ ($[K^+]_e$) and 118 mM for the intracellular $[K^+]$ ($[K^+]_I$; Stampe et al., 1998), the Goldman equation gives essentially a straight line (not shown). A permeation model based on transition state theory may account better for the observed curvature. The simplest such model supposes a single barrier to permeation

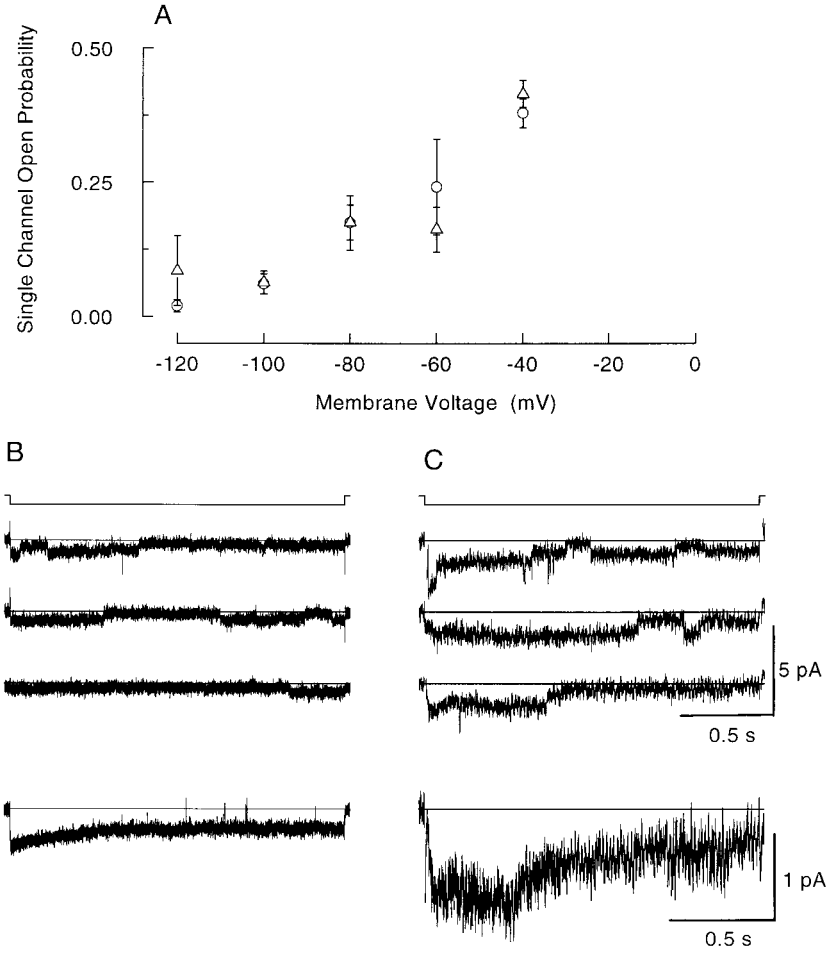

FIGURE 6 The voltage dependence of P_o (mean ± SEM) is similar for large and small Kir2.1 open levels. (*A*) Voltage dependence of open probability for the large (*circles*, $n = 5$) and the small (*triangles*, $n = 4$) open levels. (*B*) Current traces in response to hyperpolarizing steps from 0 to −80 mV (*uppermost trace*) in a mouse cardiac myocyte patch containing a single small open level (mean conductance of 4 pS). The ensemble average of 167 traces shows the inactivation process, which had a time constant of 223 ms. (*C*) Currents in response to steps from 0 to −80 mV in an HEK cell expressing Kir2.1. The patch contained two channels of ~9 pS each. The ensemble average of 12 traces is shown at the bottom. The time constant of inactivation was 342 ms.

(Jack et al., 1975, Eq. 8.24). For curve-fitting purposes a slightly modified version of the equation was used:

$$i = B\{[K^+]_i \cdot e^{(1-s)VF/RT} - [K^+]_e \cdot e^{-sVF/RT}\} \qquad (1)$$

where B is a constant that includes the amplitude of the free energy barrier, s is the position of the barrier expressed as a fraction of the potential drop across the membrane, and F, R, and T have their usual meanings. The parameters B and s were determined by fitting Eq. 1 to the *i-V* data. The best values for the large openings in Fig. 5 were 3.38 pA M^{-1} and 0.39, whereas for the small openings they were 0.77 pA M^{-1} and 0.40. The parameter B is a scaling factor, and s determines the extent of curvature in this simple model. It is clear that the degree of curvature is very similar for the large and small open levels. Only the amplitudes differ over this range of potentials.

The single barrier model allows the curvature of the large and small *i-V* relations, as measured in nearly symmetrical $[K^+]$, to be compared using a single parameter. The model is too simple, however, to explain other permeation properties of Kir2.1, including the Ussing flux ratio or the *i-V* relation in asymmetrical $[K^+]$ (Lopatin and Nichols, 1996; Stampe et al., 1998).

The small conductance openings inactivate, as do the large openings. Fig. 6 *A* compares the voltage dependence of the open probability (P_o) determined in steady-state conditions for large and small open levels. For both amplitudes P_o decreases as the membrane potential becomes more negative. Similar results have been reported by other laboratories for the I_{K1} channel in cardiac myocytes (Kameyama et al., 1983; Sakmann and Trube, 1984b). In a patch with a single small open level, recorded from a cardiac myocyte, the kinetics of voltage-dependent inactivation can be seen in the ensemble calculated from 167 individual traces (Fig. 6 *B*). The time constant for current decay from the peak to the steady-

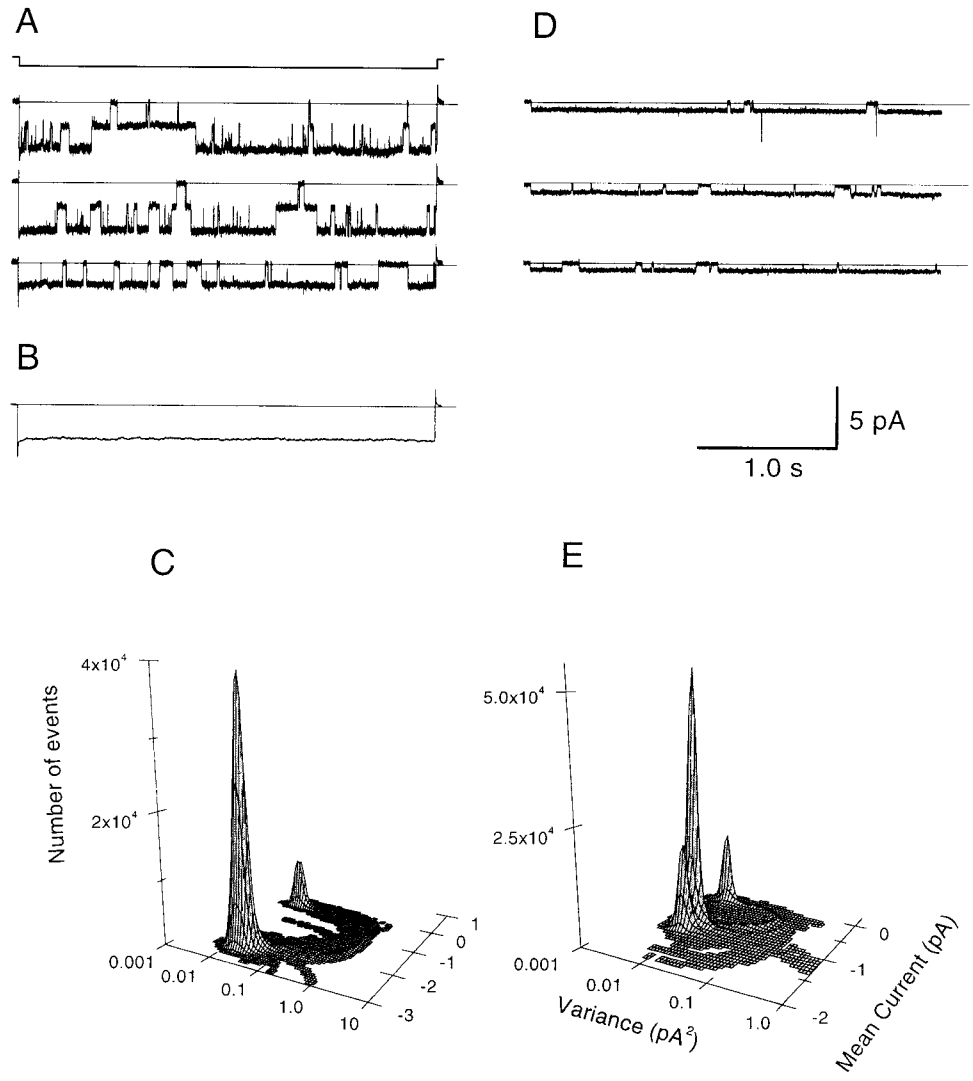

FIGURE 7 External divalent cations mediate inactivation in both large and small conductance Kir2.1 channels in the absence of external Na^+. (*A*) Cell-attached current recordings of an oocyte membrane patch with two large conductance channels (~29 pS each) in response to voltage steps from 0 to −80 mV (*uppermost trace*). The external (pipette filling) solution contained (in mM) 150 KCl, 5 Hepes, 1 EGTA, and 1EDTA. (*B*) Ensemble average of 154 pulses showing the absence of time- and voltage-dependent channel inactivation. (*C*) MV histogram analysis of single channel activity recorded in the patch shown in (*A*). The analysis was performed over 264 s when only one channel was active. The maxima correspond to the closed state and the open state (−2.34 pA); P_o is 0.80. (*D*, *E*) A small conductance channel observed in a different oocyte patch and under the same experimental conditions as in (*A*). The individual traces are 3-s stretches from a continuous recording of 300 s. Each trace starts 50 ms before an opening of the channel. (*E*) MVH analysis of the single channel activity shown in (*D*). A total of 164 s of data were analyzed. The unitary conductance was 10.1 pS, and P_o was 0.86.

state level is 223 ms, comparable to those found for the large open levels in Fig. 1, 243 and 308 ms. Similar behavior was observed when Kir2.1 was expressed in HEK cells. Fig. 6 *C* shows an HEK cell patch with two small channels that displayed a decaying transient in the ensemble average. The patch was not very stable, and the noise in the average is partly due to the small number of records (12) in the ensemble. It is clear that the small openings inactivate in a manner similar to the large openings, as can be seen both in the steady-state and dynamic data.

Divalent cations and inactivation

The pipette solution used in the previous experiments contained 1 mM Ca^{2+}, which may contribute to channel inactivation (Biermans et al., 1987; Elam and Lansman, 1995). Fig. 7 *A* shows traces from a patch containing two large, active Kir2.1 channels recorded using a pipette saline containing no free Na^+, Ca^{2+}, or Mg^{2+} (150 mM KCl, 1 mM EDTA, 1 mM EGTA and 5 mM Hepes at pH 7.4). The open probability was quite high at −80 mV, and did not change perceptibly during the 3-s step. The ensemble average in

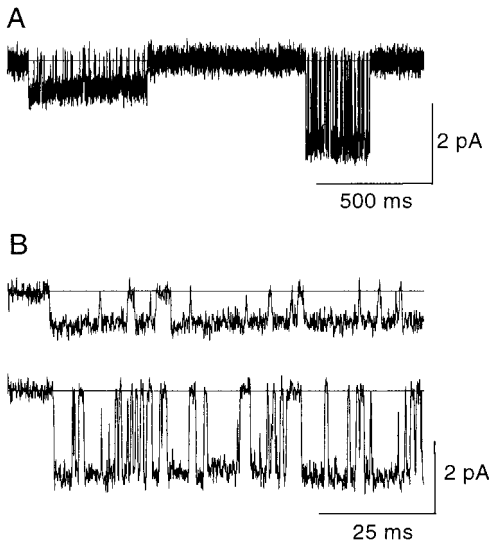

FIGURE 8 External Cs^+ blocks both large and small Kir2.1 open levels. (*A*) Small and large open levels recorded in the same patch at −80 mV. The pipette-filling solution contained 10 μM Cs^+. (*B*) Current traces with expanded time base showing the initial 180 ms after the opening of the small (*upper trace*) and large (*lower trace*) open levels shown in (*A*).

Fig. 7 *B* confirms the lack of inactivation. Although the open probability at −80 mV was the same as at 0 mV in this experiment, there are brief closures in the records. Apparently the channel can enter a closed state that differs from the inactivated one. Part way through the experiment one of the two channels became silent. Fig. 7 *C* summarizes 264 s of activity from the remaining channel; the open probability was 0.80, in contrast with the much lower values observed with 1 mM Ca^{2+} in the pipette saline (Fig. 6). The greater open probability at −80 mV gives a much larger open state peak in the MV histogram, compared to experiments with Ca^{2+} in the pipette saline, e.g., Fig. 2 *D* or Fig. 3. Fig. 7, *D* and *E* shows a similar experiment and a similar result for a single small conductance channel. The open probability for the small channel was 0.86. These findings are consistent with those reported by Elam and Lansman (1995) for Kir channels in bovine aortic endothelial cells. In summary, the P_o of both large and small Kir2.1 open levels increases when divalent cations are absent from the external solution.

Cesium blockade

Cesium ion is known to block I_{K1} in cardiac myocytes and in Kir2.1 expressed in oocytes (Isenberg, 1976; Sakmann and Trube, 1984b; Matsuda et al., 1989; Kubo et al., 1993; Abrams et al., 1996; Thompson et al., 2000). Both large- and small-conductance Kir 2.1 channels display a characteristic flickering blockade when Cs^+ (10 μM) is included in the pipette solution (Fig. 8 *A*). The first 180 ms of the openings of the two channels shown in *A* are displayed in *B* with an expanded time scale to demonstrate individual blocking-unblocking transitions. Blocking events long enough to be resolved show that the blocked state is nonconducting. The blocking and unblocking transitions are qualitatively similar for the large and small open levels, but the blocking rate seems to be higher in the case of the large openings.

To analyze the blocking kinetics quantitatively a simple model was assumed:

$$O + Cs^+ \underset{k_u}{\overset{k_b}{\leftrightarrow}} B$$

where O is the open state, B the blocked state, and k_b and k_u the rate constants of the blocking and unblocking processes, respectively. The analysis is restricted to data in which the channel flickers rapidly between open and nonconducting states, and excludes the longer closed intervals. Brief visits to closed states other than the blocked one may occur within the data analyzed, but these are expected to be infrequent compared to the closures due to Cs^+ block (cf. Figs. 1 and 8). The ratio of the rate constants, k_b/k_u, can be measured from the mean and variance of the current. From the kinetic scheme it follows that

$$p = k_u/(k_u + k_b[Cs^+]) \quad (2)$$

$$q = k_b[Cs^+]/(k_u + k_b[Cs^+]) \quad (3)$$

where p is the open probability, q is the blocked probability, and $[Cs^+]$ is the external Cs^+ concentration. For a patch with N independent and identical channels with unitary current i, the mean current I and the variance σ^2 are determined from the binomial distribution to be:

$$I = Nip \quad (4)$$

$$\sigma^2 = Ni^2pq \quad (5)$$

For a single channel

$$\sigma^2/I^2 = q/p \quad (6)$$

Substituting using Eqs. 1 and 2 gives

$$\sigma^2/I^2 = [Cs^+]k_b/k_u \quad (7)$$

Table 1 summarizes these measurements of the ratio $[Cs^+]$ k_b/k_u for four small and four large channels; the ratio is ~2.6-fold higher for the large channels than for the small ones. This result is consistent with the visual impression from Fig. 8 that Cs^+ blocks the large open level more frequently than the small one.

The values of k_b and k_u can be determined by combining the ratio of the rate constants with other kinetic information, such as the time constant or corner frequency of block, assuming the same kinetic scheme as above. The corner frequency of the block was measured by spectral analysis of the current fluctuations in single open levels in the presence of Cs^+. Fig. 9, *A* and *C* show flickering open channel

TABLE 1 Parameters of Cs^+ block at −80 mV

Unitary Conductance (pS)	Small Conductance 9.4 ± 3.7 (SEM) (n = 4)	Large Conductance 32.8 ± 2.9 (SEM) (n = 4)
f_c (Hz)	379.0 ± 55.9	571.8 ± 71.7*
$k_b[Cs^+]/k_u$	0.162 ± 0.014	0.419 ± 0.035†
k_b (M^{-1} s^{-1})	$3.3 \pm 0.6 \times 10^7$	$10.6 \pm 1.5 \times 10^{7\dagger}$
k_u (s^{-1})	2049.2 ± 301.8	2534.6 ± 323.7‡

The symbols are defined in the text.
*Significantly different (independent student's t-test $p < 0.05$).
†Significantly differnt (t-test $p < 0.005$).
‡Not significantly different (t-test $p > 0.25$).

currents of a large open level (*upper trace*), a small open level (*middle trace*), and the background noise (closed channel, *lower trace*) in the same patch, in the presence or absence of 10 μM Cs^+. Fig. 9, *B* and *D* are the associated current spectral density functions. In the absence of Cs^+, the spectra of large and small open levels both exhibit a $1/f$ characteristic, consistent with the lack of gating transitions in the open channel (Fig. 9 *D*). For both large and small open levels in Cs^+, the spectral density function follows a composite behavior: at frequencies below ~40 Hz the experimental points follow the $1/f$ spectral form. At higher frequencies the spectral density is described by a single Lorentzian component due to transitions between the open and blocked states. The spectra were fit to the equation

$$S(f) = k(1/f) + S_0/\{1 + (f/f_c)^2\} + S_h \quad (8)$$

where k determines the amplitude of the $1/f$ component, S_0 is the zero frequency asymptote of a Lorentzian component with half-power frequency, or corner frequency, f_c, and S_h is the asymptotic plateau level at high frequencies due to background noise. The average corner frequencies were 572 and 379 Hz, respectively, for four large and four small open levels (Table 1).

The corner frequency (f_c) is related to the rate constants k_b and k_u by the expression

$$f_c = \{[Cs^+]k_b + k_u\}/2\pi \quad (9)$$

Eqs. 7 and 9 can be combined to give

$$k_u = 2\pi f_c/(1 + \sigma^2/I^2) \quad (10)$$

$$k_b = 2\pi f_c(1/[Cs^+])/(1 + I^2/\sigma^2) \quad (11)$$

which express the rate constants in terms of measurable quantities. The rate constant for Cs^+ block of the large conductance levels, $10.6 \cdot 10^7$ M^{-1} s^{-1}, is 3.2 times that of the small conductance levels, $3.3 \cdot 10^7$ M^{-1} s^{-1} (Table 1). This ratio is very close to that of the average conductances of the large and small channels, 3.5 (Table 1). In contrast, the unblocking rates for the large and small levels are quite similar, 2535 and 2049 s^{-1}, respectively. In summary, the small open levels are blocked by external Cs^+ in an all-or-none manner, as are the large open levels. The unblocking rate constants are similar for the large and small open levels, but the blocking rate constant is about three times greater for large open levels.

DISCUSSION

It is widely accepted that ion channels have a main open state, the conductance of which is characteristic for a given channel type. It is surprising, therefore, that Kir2.1 channels expressed in *Xenopus* oocytes or HEK cells display a broad distribution of unitary conductances. In *Xenopus* oocytes the largest observed conductance amplitude was ~30 pS, but there were a substantial number of observations ranging down to 2 pS. Two picosiemens is near the limit of detection in these experiments, and it is possible that smaller open levels would be seen if the sensitivity of the measurements were greater. One possible interpretation is that the smaller conductance channels are background channels in oocytes or HEK cells, and not related to Kir2.1. A series of experiments comparing the biophysical properties of open levels of different sizes confirmed, however, that they are quite similar. The different sized openings display inward rectification in that the openings are seen at hyperpolarized potentials, but not at depolarized potentials. The current-voltage relations of open levels arbitrarily chosen from the upper and lower ends of the amplitude distribution both show a slight inward curvature, and the degree of curvature is similar for the large and small channels. The open levels of different size inactivate at hyperpolarized potentials, with similar voltage sensitivity, and for the different open levels the inactivation requires the presence of external cations other than K^+. Cesium ion blocks large and small open levels in an all-or-none manner, although the kinetics differ slightly. These results indicate that the channels of different conductances are related biochemically, and make it quite unlikely that some are background channels endogenous to the cell. This view is consistent with the results of control experiments on sham-injected oocytes and untransfected HEK cells, in which no inward rectifier channels were observed.

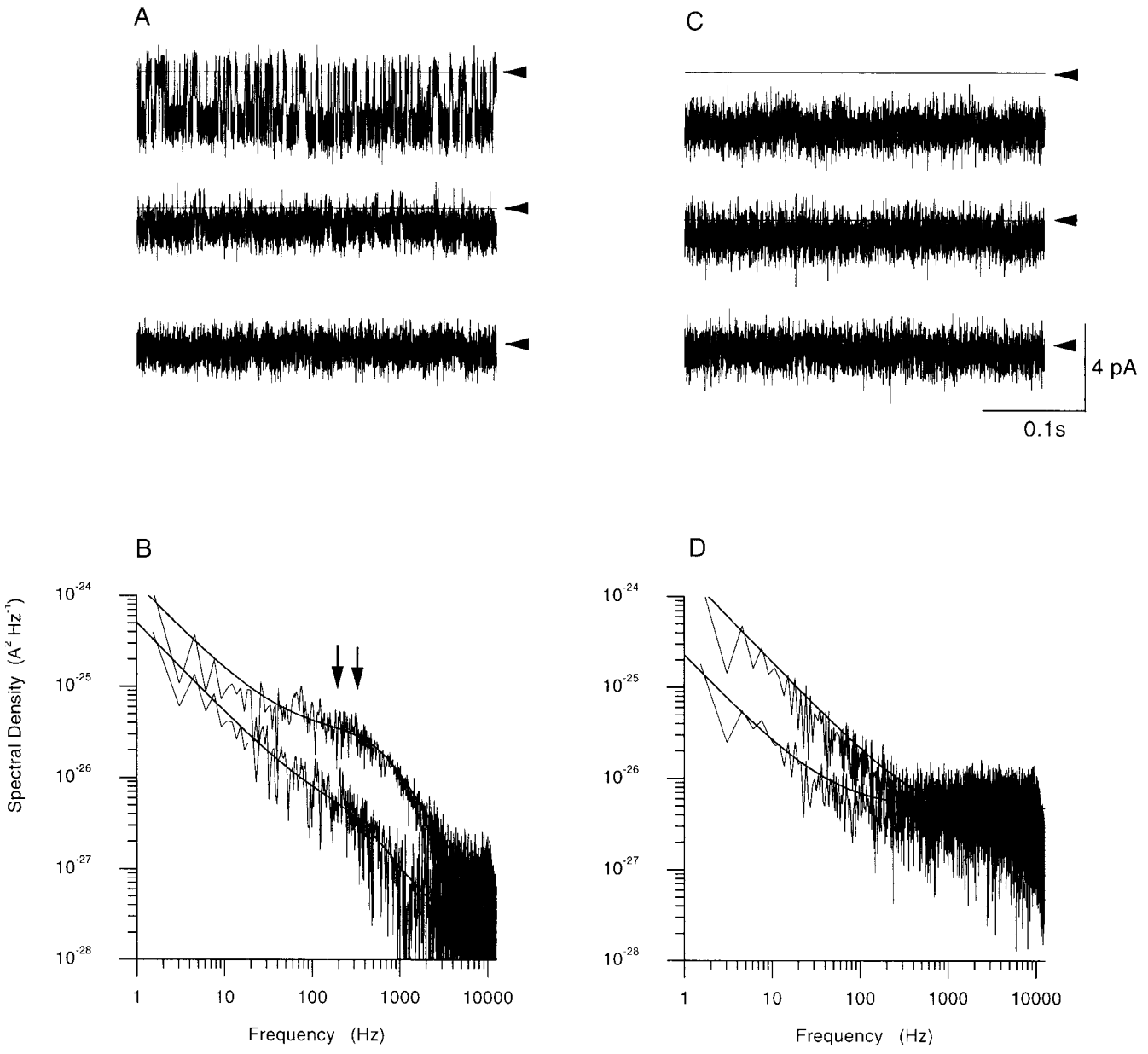

FIGURE 9 Spectral analysis of open channel current fluctuations of Kir2.1. (*A*) Examples of 350-ms stretches during openings of a large conductance channel (*upper trace*), a small conductance channel (*middle trace*) and background noise (closed state, *lower trace*) all recorded in the same patch and in the presence of 10 μM external Cs^+. Solid lines (depicted by *arrowheads*) are the zero current level. (*B*) Average difference spectral density distribution calculated for the large-conductance opening (*upper spectrum*) and the small-conductance opening (*lower spectrum*) shown in (*A*). Continuous lines are the sum of a $1/f$ noise component, a Lorentzian component, and a constant background component (Eq. 8 of the text) with fitted values (in $A^2\ Hz^{-1}$): $k = 1.33 \times 10^{-24}$, $S(0) = 2.98 \times 10^{-26}$, $S_h = 3.4 \times 10^{-28}$, $f_c = 676$ Hz for the large-conductance spectrum, and $k = 5.03 \times 10^{-25}$, $S(0) = 3.13 \times 10^{-27}$, $S_h = 1.33 \times 10^{-28}$, $f_c = 396$ Hz for the small-conductance spectrum. The values of the corner frequencies (f_c) are indicated by the vertical arrows. (*C*) Examples of 350-ms stretches during openings of a large-conductance channel (*upper trace*), a small-conductance channel (*middle trace*), and background noise (closed state, *lower trace*) all recorded in the same patch with no Cs^+ in the pipette. (*D*) Average difference spectra calculated for the large-conductance level (*upper spectrum*) and the small-conductance level (*lower spectrum*) shown in (*C*). In both cases the spectral distributions are described by a $1/f$ noise component and a constant background component, with fitted values of (in $A^2\ Hz^{-1}$): $k = 1.89 \times 10^{-24}$, $S_h = 2.99 \times 10^{-27}$ and $k = 0.22 \times 10^{-24}$, $S_h = 4.74 \times 10^{-27}$ for the large and small levels, respectively.

Cardiac myocytes

If the small conductance openings normally appear where Kir2.1 is expressed, they should be present in cardiac myocytes. In fact, we observed a broad distribution of conductance levels, 4 to 41 pS, in recordings from mouse cardiac myocytes. The interpretation of these openings is more problematic in myocytes, however, than in oocytes or HEK

cells. Messenger RNA for a closely related channel, Kir2.2, is also present in the heart (Takahashi et al., 1994). Takahahsi et al. report that Kir2.2 has a slightly greater unitary conductance than Kir2.1 when compared under the same experimental conditions. Antisense and knockout experiments show that Kir2.1 and Kir2.2 both contribute to I_{K1}, although Kir2.1 is more important (Nakamura et al., 1998; Zaritsky et al., in press). The interpretation of our results in mouse cardiac myocytes depends on whether Kir2.1 and Kir2.2 form separate homotetrameric channel populations, or form heteromeric channels. If there are two homomeric channel populations, then the conductances ranging from 2 to 35 pS may be Kir2.1 channels, as we saw in oocytes and HEK cells, whereas the ~40-pS channels would be Kir2.2 (Fig. 4 *A*). If heteromeric channels occur, however, the broad distribution of unitary conductances could result from the presence of channels differing in subunit stoichiometry. When they are co-expressed in HEK cells, Kir2.1 and Kir2.2 form homomeric, but not heteromeric, channels (Tinker et al., 1996). For the native channels, in contrast, this question is at the present unsettled, and there is some possibility that heteromeric Kir2.1/Kir2.2 channels occur in cardiac muscle (Zaritsky et al., in press).

Other known cardiac inward rectifiers are unlikely to be confused with Kir 2.n channels in these experiments. K_{ATP} channels are present in cardiac myocytes, but are generally inactive in cell-attached patches and are more flickery than the I_{K1} channels. K_{ACH} channels are expected to be present in atrial cells, but ventricular cells dominate the population of dispersed myocytes studied here; furthermore, acetylcholine was not present in the pipette.

Other laboratories studying I_{K1} have also reported multiple unitary conductances in a given species. In guinea pig, rat, and rabbit cardiac myocytes, unitary conductances of 25–47 pS have been reported, but similar inwardly rectifying channels with smaller conductances were also observed in each of these studies (Kameyama et al., 1983; Sakmann and Trube, 1984a; Payet et al., 1985; Josephson and Brown, 1986). In addition, small and large inward rectifier channels have been observed in other cell types that express Kir2.1, including skeletal muscle and corneal epithelial cells (Matsuda and Stanfield, 1989; Rae and Shepard, 1998). As in the heart, the smaller conductance openings are seen in the same conditions, and often in the same patches, as the larger openings. The simplest interpretation of all these results is that Kir2.1, whether expressed as a naturally occurring channel or in a heterologous system, gives rise to a population of channels lacking a single, characteristic, unitary conductance.

There are several reports of channels or channel complexes displaying multiple, evenly spaced conductance levels, including Cl^- channels in *Torpedo* electroplax (Miller, 1982), a molluscan K^+ channel (Kazachenko and Geletyuk, 1984), an anion-selective channel of pulmonary epithelial cells (Krouse et al., 1986), and a K^+ channel in renal epithelial cells (Hunter and Giebisch, 1987). These authors interpret their observations as evidence for multi-barreled structures. There are also channels with multiple conductance states that do not occur in integral multiples, the different conductance states presumably resulting from different states of a single-pore channel. Examples include the GABA and glycine receptor channels on mouse spinal neurons (Hamill et al., 1983), and glutamate receptors on rat hippocampal cells (Cull-Candy and Usowicz, 1987; Jahr and Stevens, 1987). In contrast to these published reports, our results show surprisingly little evidence for peaks in the histogram of amplitudes. There is a suggestion of a peak at 27.5–30 pS, and another at 5–10 pS, but there are many observations in other bins. In the case of Kir2.1, the small conductance states accessible from the closed state are quite stable, and end in returns to the closed state, giving rise to long lasting openings that are much less than the maximal conductance observed in other Kir2.1 channels.

Artifactual explanations

Could the broad distribution of unitary conductances be a recording artifact? It has been suggested that channels directly under the rim of a patch pipette have low observed unitary conductances due to the increased access resistance (Neher et al., 1978). Hamill et al. (1981) found that these "rim" channels were much rarer when the seal resistance exceeded 1 GΩ, as was the case in the experiments reported here. If rim channels were the explanation for our results, a high proportion of all recordings would need to be from rim channels, which seems unlikely. In an early description of acetylcholine receptor (AchR) and sodium channel expression in *Xenopus* oocytes, Methfessel et al. (1986) found single channel amplitude distributions with clear peaks and only modest amplitude variation. Methfessel et al. (1986) noted that the unitary conductances and kinetics of AchR and sodium channels implanted in oocytes were similar to those of the channels in their native cells.

Is the broad distribution of Kir2.1 unitary conductances an artifact of heterologous expression? It may be, for example, that the *Xenopus* oocyte expresses a Kir protein that combines with Kir2.1 to create channels of different subunit compositions, and hence different conductances. In fact, the oocyte expresses a G protein-regulated Kir channel that, together with Kir3.1, forms an active K_{ACh} channel (Hedin et al., 1996). This channel subunit is a member of a different subfamily of the Kir channels, however, and is not expected to form active channels with Kir2.1. Control experiments on oocytes show no inward rectification that could be confused with that due to Kir2.1, so there is no reason to expect an endogenous, constitutively active Kir channel component to be present at a significant level. Nevertheless, an inactive Kir2.1-like subunit that can combine with Kir2.1 to form an active channel cannot be ruled out. If this is the explanation, the phenomenon is not unique to *Xenopus* oocytes, as we

also found a wide range of Kir2.1 conductances in HEK cells expressing Kir2.1. The HEK cell experiments exclude the possibilities that the various open levels are somehow a consequence of damage to the cRNA during its synthesis or injection, or of the status of the oocytes.

Biological explanations

If the dispersion of unitary conductances is not artifactual, several other explanations can be considered, including the possibility that the channel comprises three or four protochannels (Sakmann and Trube, 1984a; Matsuda, 1988). It does not seem likely that our results can be explained by rogue activity of protochannels, however, because our amplitude distribution (Fig. 4 *A*) does not show the expected three or four peaks, or a consistent ratio of sizes (Fig. 4 *B*). Furthermore, Matsuda and colleagues have re-interpreted earlier experiments and now favor a single-barreled channel with two Mg^{2+} binding sites, rather than a multi-barreled channel (Oishi et al., 1998).

Channels with unitary conductance $<\sim$30 pS may be due to partial block of a single pore. Lu et al. (1999) have demonstrated that attaching a charged, thiol-specific reagent covalently to one or two cysteine residues within the inner pore produces Kir2.1 channels with 27% and 54% reductions in the size of the main open state. This result was interpreted as the partial block of a single pore, and suggests that partially blocked channels might explain the small openings and subconductance states described here. However, there is no obvious candidate for the blocking ion in our experiments. The small open states are seen at very negative potentials, at which known blockers such as cytoplasmic Mg^{2+} or polyamines (Nichols and Lopatin, 1997) are unlikely to be in the channel. There was no tendency for small openings to switch directly to large openings at negative potentials, as would be expected if a charged blocker exited the channel. Small channels are also seen when the pipette saline has very low levels of Na^+, Ca^{2+}, or Mg^{2+}, which might be considered candidates for the blocking ion. The binding of the blocking molecule would have to be very tight, as the unitary conductance amplitudes were stable throughout patch recordings. If partial block is occurring, the blocking species is probably not charged.

Are the unitary conductances $<\sim$30 pS related to the transient visits to more conventional subconductance states? In channels of $\sim$30 pS we frequently observed brief visits to a substate of $\sim$¾ the main state amplitude. Less frequently, substates of $\sim$½ and $\sim$¼ γ were seen. This behavior of Kir2.1 in oocytes is quite similar to that described by Sakmann and Trube (1984a) for cardiac Kir channels. Thus, perhaps the channel can open directly to one of three subconductance states. The amplitude histogram for Kir2.1, however, does not show the expected peaks. Furthermore, the subconductance states accessible from the main open state, e.g., the ¾ γ substate, are quite brief. In contrast, the small and intermediate-sized openings from the closed state are much longer, and are the main open states for those channels. Thus the subconductance states accessible from the open state appear to be unrelated to the small- and intermediate-conductance main open states of these channels.

The only biophysical difference we detected between the $\sim$30 pS channels and the smaller ones is the reduced rate constant for block by Cs^+ in the small-conductance channels. The extent of the reduction was strongly correlated with the amplitude of the unitary K^+ currents (Table 1). In all these experiments, including those without external Cs^+, the unitary conductances were measured 60 to 120 mV negative to the K^+ equilibrium potential, where the net K^+ flux was almost entirely due to inward flux. The reduction in the rate constant for Cs^+ block is then perhaps not surprising: the rate of K^+ entry for the channels smaller than $\sim$30 pS is reduced compared to the $\sim$30 pS channels, and the entry rate for another monovalent cation, Cs^+, is reduced to a similar extent in the same channels. Thompson et al. (2000) have recently shown that Cs^+ blocks Kir2.1 channels by binding a site on the cytoplasmic side of the selectivity filter. Thus it is natural to interpret the Cs^+ block experiments as follows. A cesium ion enters the channel from the external (pipette) solution, passes through the selectivity filter and binds at a site or sites at the end of the filter, or just beyond it, with the residues of serine 165 and threonine 141 contributing to the binding site(s) (Thompson et al., 2000). The ion remains on the binding site, blocking K^+ permeation for 400 to 500 μs on average, then leaves the site and continues on through the channel and into the cytoplasm. The first part of the pathway, from the external saline to the Cs^+ binding site, varies for some reason among individual channels and causes parallel changes in the entry rates for Cs^+ and K^+. The rate constant for the Cs^+ unblocking reaction is very similar for the large and small conductance channels, indicating that the pathway from the Cs^+ binding site to the cytoplasm is also similar for these channels. Thus the differences in the unitary conductances among the individual channels seem to lie external to the Cs^+ binding site, i.e., on the extracellular surface of the protein, in the outer pore, or in the selectivity filter itself.

The variation in unitary conductance occurs in channels synthesized from a single mRNA species in the oocyte experiments, or a single cDNA species in the HEK cell experiments, making it very unlikely that the channels differ in primary structure. The conductance levels are stable for as long as we have been able to observe them, suggesting that perhaps a covalent modification of the channel is responsible for the different conductance amplitudes. Covalent modifications such as phosphorylation or ADP ribosylation seem unlikely on the extracellular domains of the channel protein. Variation in the nature or extent of glycosylation, in contrast, may provide a mechanism. The sialic acid groups present in asparagine-linked complex oligosac-

charides supply a negative charge that could influence the local concentration of extracellular cations, and hence alter K^+ or Cs^+ influx. Recio-Pinto et al. (1990) have in fact shown that removal of sialic acid by neuroaminidase digestion alters the unitary conductance of electroplax Na^+ channels. Taking the KcsA potassium channel structure as a model for Kir2.1, the potentially extracellular Kir2.1 peptide sequence lies between the carboxyl end of the outer helix and the amino end of the inner helix (Doyle et al., 1998). This region contains an asparagine residue at amino acid position 127, which is a candidate for N-linked glycosylation. Whatever the biochemical mechanism, the range of unitary conductances observed in single Kir2.1 channels (2–~30 pS) is quite large. If the mechanism is under cellular control, the regulation of inward rectifier current density at the level of the unitary conductance could have a major influence on Kir current density, and thus electrical excitability, at the whole-cell level.

We thank Robert Berg for technical help and Dr. Juan Korenbrot, in whose laboratory some of these experiments were carried out. We also thank Dr. Jenny A. Visser and Dr. Christophe Paillart for their help with the cell transfection experiments.

This work was supported in part by the Department of Veterans Affairs.

REFERENCES

Abrams, C. J., N. W. Davies, P. A. Shelton, and P. R. Stanfield. 1996. The role of a single aspartate residue in ionic selectivity and block of a murine inward rectifier K^+ channel Kir2.1. *J. Physiol.* 493.3:643–649.

Anderson, C. R., and C. F. Stevens. 1973. Voltge-clamp analysis of acetylcholine produced end-plate current fluctuations at frog neuromuscular junction. *J. Physiol.* 235:655–691.

Biermans, G., J. Vereecke, and E. Carmeliet. 1987. The mechanism of the inactivation of the inward-rectifying K current during hyperpolarizing steps in guinea-pig ventricular myocytes. *Pflugers Arch.* 410:604–613.

Colquhoun, D., and A. G. Hawkes. 1977. Relaxation and fluctuations of membrane currents that flow through drug-operated ion channels. *Proc. R. Soc. Lond. (B.)* 199:231–262.

Colquhoun, D., and F. J. Sigworth. 1995. Fitting and statistical analysis of single-channel records. *In* Single-Channel Recording, 2nd Ed. B. Sakmann and E. Neher, editors. Plenum Press, New York. 483–588.

Conti, F., and E. Wanke. 1975. Channel noise in nerve membranes and lipid bilayers. *Q. Rev. Biophys.* 8:451–506.

Cull-Candy, S. G., and M. M. Usowicz. 1987. Multiple-conductance channels activated by excitatory amino acids in cerebellar neurons. *Nature.* 325:525–528.

Doyle, D. A., J. Morais Cabral, R. A. Pfuetzner, A. Kuo, J. M. Gulbis, S. L. Cohen, B. T. Chait, and R. MacKinnon. 1998. The structure of the potassium channel: molecular basis of K^+ conduction and selectivity. *Science*. 280:69–77.

Elam, T., and J. B. Lansman. 1995. The role of Mg^{2+} in the inactivation of inwardly rectifying K^+ channels in aortic endothelial cells. *J. Gen. Physiol.* 105:463–484.

Fox, J. A. 1987. Ion channel subconductance states. *J. Membr. Biol.* 97:1–8.

Hamill, O. P., J. Bormann, and B. Sakmann. 1983. Activation of multiple-conductance state chloride channels in spinal neurones by glycine and GABA. *Nature.* 305:805–808.

Hamill, O. P., A. Marty, E. Neher, B. Sakmann, and F. J. Sigworth. 1981. Improved patch clamp techniques for high-resolution current recording from cells and cell-free membrane patches. *Pflugers Arch.* 391:85–100.

Hedin, K. E., N. F. Lim, and D. E. Clapham. 1996. Cloning of a *Xenopus laevis* inwardly rectifying K^+ channel subunit that permits GIRK1 expression of I_{KACh} currents in oocytes. *Neuron.* 16:423–429.

Hunter, M., and G. Giebisch. 1987. Multi-barreled K channels in renal tubules. *Nature.* 327:522–524.

Isenberg, G. 1976. Cardiac Purkinje fibers. Cesium as a tool to block inward rectifying potassium currents. *Pflugers Arch.* 391:99–106.

Ishihara, K., and M. Hiraoka. 1994. Gating mechanism of the cloned inward rectifier potassium channel from mouse heart. *J. Membr. Biol.* 142:55–64.

Jack, J. J. B., D. Noble, and R. W. Tsien. 1975. Electric current flow in excitable cells. Clarendon Press, Oxford.

Jahr, C., and C. F. Stevens. 1987. Glutamate activates multiple single channel conductances in hippocampal neurons. *Nature.* 325:522–525.

Josephson, I. R., and A. M. Brown. 1986. Inwardly rectifying single-channel and whole cell K^+ currents in rat ventricular myocytes. *J. Membr. Biol.* 94:19–35.

Kameyama, M., T. Kiosue, and M. Soejima. 1983. Single channel analysis of the inward rectifier K current in the rabbit ventricular cells. *Jpn. J. Physiol.* 33:1039–1056.

Katz, B., and R. Miledi. 1972. The statistical nature of the acetylcholine potential and its molecular components. *J. Physiol.* 224:665–699.

Kazachenko, V. N., and V. I. Geletyuk. 1984. The potential-dependent potassium channel in molluscan neurons is organized in a cluster of elementary channels. *Biochim. Biophys. Acta.* 773:132–142.

Krouse, M. E., G. T. Schneider, and P. W. Gage. 1986. A large anion-selective channel has seven conductance levels. *Nature.* 319:58–60.

Kubo, Y., T. J. Baldwin, Y. N. Jan, and L. Y. Jan. 1993. Primary structure and functional expression of a mouse inward rectifier potassium channel. *Nature.* 362:127–132.

Lopotin, A. N., and C. G. Nichols. 1996. $[K^+]$ dependence of open-channel conductance in cloned inward rectifier potassium channels. *Biophys. J.* 71:682–694.

Lu, T., B. Nguyen, X. Zhang, and J. Yang. 1999. Architecture of a K^+ channel pore revealed by stoichiometric covalent modification. *Neuron.* 22:571–580.

Matsuda, H. 1988. Open-state structure of inwardly rectifying potassium channels revealed by magnesium block in guinea-pig heart cells. *J. Physiol.* 397:237–258.

Matsuda, H., and P. R. Stanfield. 1989. Single inwardly rectifying potassium channels in cultured muscle cells from rat and mouse. *J. Physiol.* 414:111–124.

Matsuda, H., H. Matsuura, and A. Noma. 1989. Triple-barrel structure of inwardly rectifying K^+ channels revealed by Cs^+ and Rb^+ block in guinea-pig heart cells. *J. Physiol.* 413:139–157.

Methfessel, C., V. Witzemann, T. Takahashi, M. Mishina, S. Numa, and B. Sakmann. 1986. Patch clamp measurements on *Xenopus laevis* oocytes: currents through endogenous channels and implanted acetylcholine receptor and sodium channels. *Pflugers Arch.* 407:577–588.

Miller, C. 1982. Open-state substructure of single chloride channels from Torpedo electroplax. *Phil. Trans. R. Soc. B. Biol. Sci.* 299:401–411.

Nakamura, T. Y., M. Artman, B. Rudy, and W. A. Coetzee. 1998. Inhibition of rat ventricular I_{K1} with antisense oligonucleotides targeted to Kir2.1 mRNA. *Am. J. Physiol. Heart Circ. Physiol.* 274:H892–H900.

Neher, E., B. Sakmann, and J. H. Steinbach. 1978. The extracellular patch clamp: a method for resolving currents through individual open channels in biological membranes. *Pflugers Arch.* 375:219–228.

Neher, E., and C. F. Stevens. 1977. Conductance fluctuations and ion pores in membranes. *Annu. Rev. Biophys. Bioeng.* 6:345–381.

Nichols, C. G., and A. N. Lopatin. 1997. Inward rectifier potassium channels. *Annu. Rev. Physiol.* 59:171–191.

Oishi, K., K. Omori, H. Ohyama, K. Shingu, and H. Matsuda. 1998. Neutralization of aspartate residues in the murine inwardly rectifying K^+

channel IRK1 affects the substate behavior in Mg^{++} block. *J. Physiol.* 510:3:675–683.

Patlak, J. B. 1993. Measuring kinetics of complex single ion channel data using mean-variance histograms. *Biophys. J.* 65:29–42.

Payet, M. D., E. Rousseau, and R. Sauve. 1985. Single-channel analysis of a potassium inward rectifier in myocytes of newborn rat heart. *J. Membr. Biol.* 86:79–88.

Plaster, N. M., R. Tawil, M. Tristani-Firouzi, S. Canun, S. Bendahhou, A. Tsunoda, M. R. Donaldson, S. T. Iannaccone, E. Brunt, R. Barohn, J. Clark, F. Deymeer, A. L. George, F. A. Fish, A. Hahn, A. Nitu, C. Ozdemir, P. Serdaroglu, S. H. Subramony, G. Wolfe, G. Y.-H. Fu, and L. J. Ptacek. 2001. Mutations in Kir2.1 cause the developmental and episodic electrical phenotypes of Anderson's syndrome. *Cell.* 105: 511–519.

Rae, J. L., and A. R. Shepard. 1998. Inwardly rectifying potassium channels in lens epithelium are from the IRK1 (Kir2.1) family. *Exp. Eye Res.* 66:347–359.

Recio-Pinto, E, W. B. Thornhill, D. S. Duch, S. R. Levinson, and B. W. Urban. 1990. Neuraminidase treatment modifies the function of electroplax sodium channels in planar lipid bilayers. *Neuron.* 5:675–684.

Sakmann, B., and G. Trube. 1984a. Conductance properties of single inwardly rectifying potassium channels in ventricular cells from guinea-pig heart. *J. Physiol.* 347:641–657.

Sakmann, B., and G. Trube. 1984b. Voltage-dependent inactivation of inward-rectifying single-channel currents in the guinea-pig heart cell membrane. *J. Physiol.* 347:659–683.

Stampe, P., J. Arreola, P. Perez-Cornejo, and T. Begenisich. 1998. Non-independent K^+ movement through the pore in IRK1 potassium channels. *J. Gen. Physiol.* 112:475–484.

Takahashi, N., K-I. Morishige, A. Jahangir, M. Yamada, I. Findley, H. L. Koyama, and Y. Kurachi. 1994. Molecular cloning and functional expression of cDNA encoding a second class of inward rectifier potassium channels in the mouse brain. *J. Biol. Chem.* 269: 23274–23279.

Thompson, G. A., M. L. Lyeland, I. Ashmole, M. J. Sutcliffe, and P. R. Stanfield. 2000. Residues beyond the selectivity filter of the K+ channel Kir2.1 regulate permeation and block by external Rb+ and Cs+. *J. Physiol.* 526.2:231–240.

Tinker, A., Y. N. Jan, and L. Y. Jan. 1996. Regions responsible for the assembly of inwardly rectifying potassium channels. *Cell.* 87:857–868.

Zaritsky, J. J., J. B. Redell, B. L. Tempel, and T. L. Schwarz. 2001. The consequences of disrupting cardiac I_{K1} as revealed by the targeted deletion of the murine Kir2.1 and Kir2.2 genes. *J. Physiol.* in press.

Zhu, G., Zhang, Y., Xu, H., and C. Jiang. 1998. Identification of endogenous outward currents in the human embryonic kidney (HEK293.) cell line. *J. Neurosci. Meth.* 81(1–2):73–83.